IEEE Access
Multidisciplinary | Rapid Review | Open Access Journal

Received January 2, 2019, accepted January 11, 2019, date of publication January 18, 2019, date of current version March 7, 2019.

Digital Object Identifier 10.1109/ACCESS.2019.2893347

Design of Frequency-Selective Rasorbers Based on Centrosymmetric Bended-Strip Resonator

MIN GUO, ZHANSHAN SUN, DI SANG, XUEQING JIA, AND YUNQI FU
College of Electronic Science, National University of Defense Technology, Changsha, China

Corresponding author: Yunqi Fu (yunqifu@nudt.edu.cn)

This work was supported in part by the National Natural Science Foundation of China under Grant 61571448.

ABSTRACT Two frequency-selective rasorber (FSR) structures using novel centrosymmetric bended-strip resonator (CBSR) are proposed in this paper. Both FSRs consist of the resistive sheet layer and the bandpass FSS layer with an air gap in the middle. The resistive sheet layer is constructed by inserting the CBSR into the center of the resistor-loaded dipole. The CBSR resonates at the transmission band of the bandpass FSS and exhibits infinite impedance, which is used to realize high-transmittance performance at the transmission band. The full wave simulation results show that the transmission band of one FSR is above the absorption band (A-T FSR), while the transmission band of another FSR is below the absorption band (T-A FSR). The transmission band of the A-T FSR and T-A FSR are separately located at 12.76 and 6.08 GHz with 0.66- and 0.13-dB insertion loss, and the corresponding absorption bands with absorption rate >90% are located at 6.10–10.98 GHz and 9.04–15.94 GHz, respectively. The CBSR used in T-A FSR (M-CBSR) is a miniaturized design of the CBSR used in A-T FSR. Comparing with the CBSR structure, the electric length of the M-CBSR's longer side is reduced to about 50%, which is only 12.2% of the wavelength of the transmission band. Two prototypes are fabricated and measured to verify the absorption/transmission performance of the proposed FSRs. The measured results are in good agreements with simulated results, which evidently demonstrates the validity of the proposed design.

INDEX TERMS Frequency-selective rasorber (FSR), centrosymmetric bended-strip resonator, transmission band below the absorption band, transmission band above the absorption band.

I. INTRODUCTION

Frequency selective surface (FSS) radome has been studied for decades, it allows electromagnetic waves to transmit in the transmission band and reflects the electromagnetic wave out-of-band [1]–[3]. Although the antenna mono-static radar cross section (RCS) reduces sharply, the bistatic RCS may increase. To get better RCS reduction, the frequency-selective rasorber (FSR) radome with absorption performance is proposed [4]. The word ''rasorber'' is a combination of the words ''radome'' and ''absorber''.

Many different FSRs have been reported [5]–[15] in recent years. They can be divided into three categories according to the relationship between absorption and transmission band: transmission band below the absorption band (T-A FSR) [5]–[7], absorption band below the transmission band (A-T FSR) [8]–[10], and two absorption bands at both sides of the transmission band (A-T-A FSR) [11]–[15]. These FSRs are very useful for antenna stealth due to the absorptive performance.

In general, the FSR consists of the resistive sheet layer and the bandpass FSS layer. When the lossless bandpass FSS is used at the bottom layer, the insertion loss of the transmission band is only decided by the impedance of the resistive sheet layer. Infinite impedance of the resistive layer brings about the high-transmittance performance [10]. Therefore, the equivalent parallel LC resonance structure in the resistive sheet layer is usually used to realize infinite impedance, and many researchers focus on the design of the resonance structures in recent years [5]–[15]. These FSRs with different resonance structures work in the different transmission band with the high-transmittance performance, and they have excellent broadband absorption properties out of the transmission band.

One of the effective parallel LC resonance structures is bended-strip resonator (BSR), which is used to design the A-T FSR [9] and the A-T-A FSR [12]. Inspired by above BSR structure, the centrosymmetric bended-strip resonator (CBSR) is proposed in this paper firstly. Since the resonance frequency is mainly decided by the BSR's longer side. Often, the length of the BSR's longer side is about one fourth of the wavelength of the transmission band. When the transmission band shifts to the lower frequency, especially the frequency of the transmission band varies greatly, the size

of the resonance structure needs to be enlarged apparently, which may lead to the grating lobe and degenerate the performance of the oblique incidence. To solve this problem, one miniaturized design is necessary. Hence, the CBSR is finely modified by connecting its two arms to achieve a miniaturized CBSR (M-CBSR). Comparing with the CBSR structure, the electric length of the M-CBSR's longer side is reduced about 50%, which is only 12.2% of the wavelength of the transmission band. The CBSR and M-CBSR are used to design A-T FSR and T-A FSR with high-transmittance performance, respectively.

At first, the A-T FSR using CBSR is introduced. The transmission band of the A-T FSR is located at 12.76GHz with 0.66dB insertion loss, and the absorption band with the absorption rate $>$ 80% extends from 5.53GHz to 11.5GHz. Then, the T-A FSR is introduced. The transmission band of the T-A FSR using M-CBSR is located at 6.08GHz with 0.13dB insertion loss, and the absorption band with the absorption rate $>$ 80% extends from 8.47GHz to 16.0GHz. Both FSRs consist of dual-layer structures with an air gap in the middle. The resistive sheet layer is in the upper layer. The lossless FSS is located at the bottom. Two resonant structures (CBSR and M-CBSR) are placed at the center of the resistive sheet layer to resonate at the transmission band and exhibit infinite impedance. Two slot-type square FSSs with different size are used to match the transmission bands with the resistive sheet layer. The metallic dipole loaded with lumped resistors is used to generate a wide absorption band. For a demonstration, two prototypes are fabricated. The performance of the proposed structure is measured by a parallel-plate waveguide (PPW) measurement. Measured and simulated results are in good agreement, which shows the validity of the proposed design.

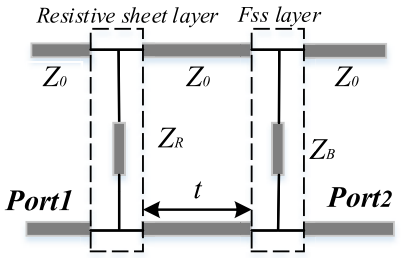

FIGURE 1. The equivalent circuit model of the dual-layered structure.

II. THE IMPORTANCE OF EQUIVALENT PARALLEL LC RESONATOR

The dual-layered structure can be equivalent to a two-port network, which is shown in Fig.1. Z_R and Z_B denote the equivalent impedances of the resistive sheet layer and the bandpass FSS layer. Z_0 is the characteristic impedance of free space. The two-layered structure is separated by an air gap in the middle, so the impedance between the resistive sheet layer and the bandpass FSS layer is Z_0. According to the equivalent circuit model, the ABCD matrix of the dual-layered structure is:

$$\begin{aligned}
&\begin{bmatrix} A & B \\ C & D \end{bmatrix} \\
&= \begin{bmatrix} 1 & 0 \\ \frac{1}{Z_R} & 1 \end{bmatrix} \begin{bmatrix} \cos\beta t & jZ_0 \sin\beta t \\ j\frac{\sin\beta t}{Z_0} & \cos\beta t \end{bmatrix} \begin{bmatrix} 1 & 0 \\ \frac{1}{Z_B} & 1 \end{bmatrix} \\
&= \begin{bmatrix} \cos\beta t + j\frac{Z_0}{Z_B}\sin\beta t & jZ_0\sin\beta t \\ \frac{Z_R+Z_B}{Z_R Z_B}\cos\beta t + j(\frac{1}{Z_0}+\frac{Z_0}{Z_R Z_B})\sin\beta t & \cos\beta t + j\frac{Z_0}{Z_R}\sin\beta t \end{bmatrix}
\end{aligned} \tag{1}$$

where $\beta = 2\pi/\lambda$. So the transmission coefficient between the two ports can be calculated as follows:

$$\begin{aligned}
|S_{21}| &= \frac{2}{\left|A + \frac{B}{Z_0} + CZ_0 + D\right|} \\
&= \frac{2}{\left|\left(2 + \frac{Z_0(Z_R+Z_B)}{Z_R Z_B}\right)\cos\beta t + j\left(2 + \frac{Z_0(Z_R+Z_B+Z_0)}{Z_R Z_B}\right)\sin\beta t\right|}
\end{aligned} \tag{2}$$

The lossless bandpass FSS used at the bottom layer generates parallel resonance at the transmission band. So that $Z_B \to \infty$ at the transmission band. The transmission coefficient could be simplified as follows:

$$|S_{21}| = \frac{2}{\left|\left(2 + Z_0/Z_R\right)(\cos\beta t + j\sin\beta t)\right|} = \frac{2}{\left|\left(2 + Z_0/Z_R\right)\right|} \tag{3}$$

Eq. (3) indicates that the insertion loss of the two-layered FSR is mainly determined by Z_R. The perfect transmission band with least insertion loss (S21 = 1) can be obtained by infinite impedance. It should be pointed out that the insertion loss decreases with the impedance increasing. Therefore, the design of the resistive sheet layer is very important to the low insertion loss.

Considering the FSR structure proposed in this paper, the resistive sheet layer using the metallic dipole loaded with lumped resistors is similar to the design in [8], [9], and [11]. The equivalent circuit model of the resistor-loaded dipole is series *RLC*. As the impedance of the series *RLC* is finite, the equivalent parallel LC resonator at the center of the resistive sheet layer is the key point to realize infinite impedance. Therefore, the design of the resonator is the most important part to realize the transmission band with high-transmittance performance.

This paper focuses on the design of equivalent parallel LC resonator and its miniaturized design. CBSR and M-CBSR are proposed. Meanwhile, they are used to construct two FSRs with high-transmittance performance, as explained in the following section.

III. DESIGN AND ANALYSIS OF THE PROPOSED FSRS USING CBSR AND M-CBSR

Both FSRs consist of dual-layer structures with an air gap in the middle. The resistive sheet layer is in the upper layer.

The FSS is located at the bottom. CBSR and M-CBSR structures are placed at the center of the resistive sheet layer to resonate at the transmission band and exhibit infinite impedance, which is used to realize high-transmittance performance. Two slot type square FSSs with different size are only designed to match the transmission bands with the resistive sheet layer. Therefore, the design and analysis of the resistive sheet layer using CBSR and M-CBSR are demonstrated firstly.

A. DESIGN AND ANALYSIS OF THE RESISTIVE SHEET LAYER USING CBSR AND M-CBSR

The resistive sheet layers with the proposed resonators are shown in Fig.2. Two resonators are placed at the center of the resistor-loaded dipole to resonate at the transmission band and exhibit infinite impedance. The M-CBSR is designed by connecting two arms of the CBSR.

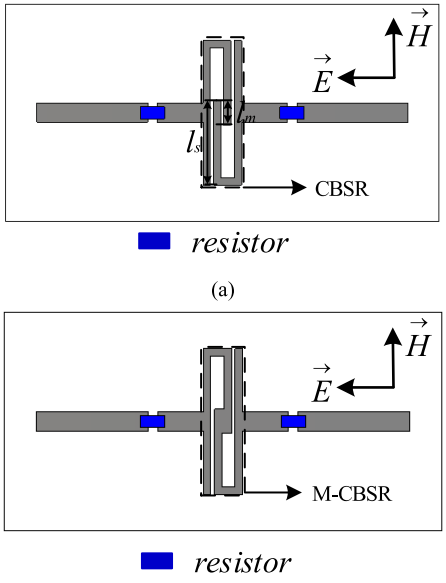

FIGURE 2. The resistive sheet layer (a) CBSR. (b) M-CBSR.

To explain the working principles of the proposed structures, equivalent circuit models (ECMs) are illustrated in Fig.3. It works along with the electric field, which is shown in Fig. 2. The impedance of the resistive sheet layer of the CBSR and M-CBSR are separately represented by Z_H and Z_L. As shown in Fig.3 (a) and (b), Z_H and Z_L can be calculated as follows:

$$Z_H = (R + jwL + 1/jwC) + Z_c \tag{4}$$

$$Z_c = j \cdot \frac{(C_s+C_m)(w^2L_sC_s-1)(w^2L_sC_m-1) - w^2L_sC_m^2(1+w^2L_sC_s)}{wC_m(w^2L_sC_sC_m - C_s - C_m)(1+w^2L_sC_s)} \tag{5}$$

$$Z_L = (R + jwL + 1/jwC) + 2jwL_s/(1 - wL_sC_s) \tag{6}$$

To achieve low insertion loss at the transmission band, the impedance of the two resistive sheet layers should

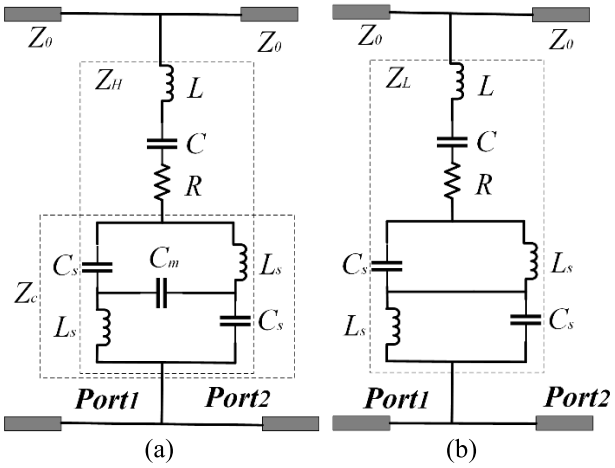

FIGURE 3. Equivalent circuit model of the resistive sheet layer. (a) CSBR. (b) M-CBSR.

be infinite. That is to say:

$$f_H = 1/2\pi\sqrt{L_s(C_sC_m/(C_s + C_m))} \tag{7}$$

$$f_L = 1/2\pi\sqrt{L_sC_s} \tag{8}$$

Since $C_s > (C_sC_m)/(C_s + C_m)$, $f_H > f_L$. As shown in Fig.2, the length of the equivalent capacitance structure outside ($l_s = 3.5$mm) is 3.5 times the equivalent capacitance length inside ($l_m = 1.0$mm). The length of the parallel-strip capacitor is proportional to the equivalent capacitance value [16]. Hence, C_s is about 3.5 times C_m. Meanwhile, the other structures are unchanged. In other words, the equivalent capacitance and inductance values of the ECMs are unchanged. $f_H = 2.12f_L$ can be deduced. It can be concluded that the resonance frequency of two resistive sheet layers with infinite impedance could be separately generated at high frequency (f_H) and low frequency (f_L).

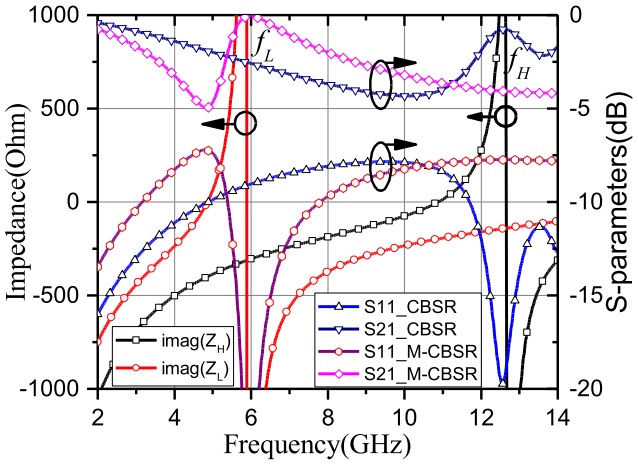

FIGURE 4. S-parameters and imaginary part of two resistive sheet layers' impedance obtained by full-wave simulation in CST.

S-parameters and imaginary part of two resistive sheet layers' impedance obtained by full-wave simulation is shown in Fig.4. When the CSBR is used at the center of the resistive

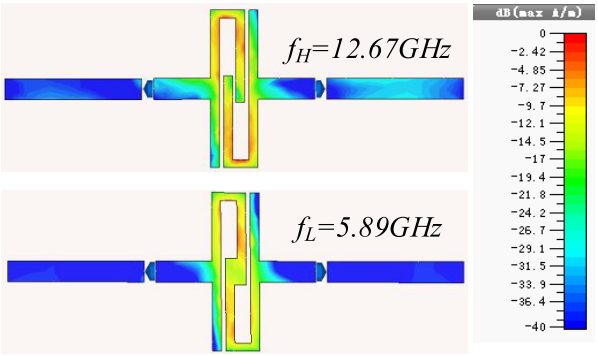

FIGURE 5. The surface current distribution on the resistive sheet layers.

sheet layer, the frequency of infinite impedance is located at $f_H = 12.67$GHz. When the M-CSBR is used, the frequencies of infinite impedance are located at $f_L = 5.89$GHz. $f_{A-T} = 2.15 f_{T-A}$. The high-transmittance bands of the resistive sheet are corresponded with the frequencies of infinite impedance. Since the impedance of the resistive sheet at f_H is smaller than that at f_L, thus the insertion loss of the resistive sheet at f_H is larger. It should be noted that the impedance of the resistive sheet is large enough to obtain high-transmission performance at f_L and f_H [15]. In summary, two resistive sheet layers using CBSR and M-CBSR can be used to design the high-transmittance FSR. By comparing the full-wave simulation results and the ECMs analysis. It can be concluded that the analysis of ECMs predicts the transmission bands of the proposed resistive sheet layer well. Fig.5 shows the surface current distribution on the resistive sheet layer using CBSR and M-CBSR at f_L and f_H. The surface current concentrates on the central resonator, which is coincided with the above analysis.

In summary, the M-CBSR can be designed by connecting two arms of the CBSR. The size of the two CBSRs is 1.5mm × 6.0mm. Although the size of the resonance structure is same. The resonance frequency of M-CBSR can shift to lower frequency. Comparing with the previous resonance structure, the resonance frequency of the proposed CBSR could shift to the lower frequency without enlarging the resonator.

IV. DESIGN AND ANALYSIS OF THE PROPOSED FSRS USING CBSR AND M-CBSR

The unit cell of the proposed FSRs is shown in Fig.6. It includes two kinds FSRs using CBSR and M-CBSR which have different transmission band. The transmission band of one FSR using CBSR is above the absorption band. It belongs to A-T FSR. The transmission band of the other FSR using M-CBSR is below the absorption band. It belongs to T-A FSR.

Each FSR consists of a resistive layer and an FSS layer. Both layers are printed on a dielectric substrate Rogers 4350B with a thickness of 0.508mm. These layers are separated by an air spacer. In the resistive sheet layers, two resonance

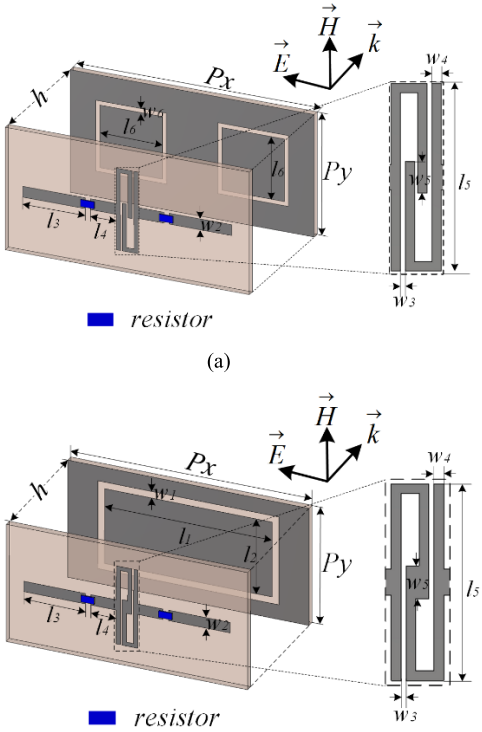

FIGURE 6. The structure of the proposed FSRs. (a) A-T FSR using CBSR. (b) T-A FSR using M-CBSR. (The geometrical parameters of the unit cell are optimized as: $Px = 18pmm$, $Py = 9mm$, $l1 = 12.5mm$, $l2 = 5.75mm$, $l3 = 4.6mm$, $l4 = 1.9mm$, $l5 = 6.0mm$, $w1 = 0.5mm$, $w2 = 0.8mm$, $w3 = 0.15mm$, $w4 = 0.3mm$, $w5 = 1.0mm$, $w6 = 0.3mm$, $h = 5mm$, $R = 160ohm$.)

structures are designed to get low insertion loss at the two transmission bands. The metallic dipoles, loaded with resistors, are used to achieve the wide absorption band. Two slot-square FSSs with different transmission bands are used at the bottom layer. The transmission bands of the FSS layer are in good agreement with the resistive sheet layer so as to achieve low insertion loss at the transmission band.

Furtherly, the simulated S-parameter results of the A-T and T-A FSRs using CST are shown in Fig.7 (a) and (b). The absorption rate of the proposed FSRs is shown in Fig.7(c). Full wave simulated results show that the transmission band of the A-T FSR using CBSR is located at 12.76GHz with 0.65dB insertion loss. The absorption band with the absorption rate $>$ 90% extends from 6.10GHz to 10.98GHz. The transmission band of the A-T FSR using M-CBSR is located at 6.08GHz with 0.13dB insertion loss. The corresponding absorption bands with absorption rate $>$ 90% are 9.04–15.94 GHz.

The reflection and transmission coefficients of the proposed FSRs under oblique incidence are shown in Fig.8. Absorption bands and transmission bands are relatively steady under the incident angle up to 30 degrees. Two transmission bands are located at 12.76GHz (f_H) and 6.08GHz (f_L). The insertion loss at the low and high transmission bands is less than 0.17dB and 0.76dB under all simulated incidence.

TABLE 1. Performance comparison of 2-D FSRs.

Ref	FSR type	Parallel LC resonator	Transmission band (f_m) /Insertion loss	Electric size(λ_m)
[9]	A-T	λ_m/4 BSR	9.74GHz/0.37dB	0.140×0.241
[10]	A-T	Dual-layer dipole	5.60GHz/0.2dB	0.189×0.302
[11]	A-T-A	Double square-loop	6.10GHz/0.3dB	0.199×0.199
This work	A-T	CBSR	12.76GHz/0.65dB	0.064×0.255
	T-A	M-CBSR	6.08GHz/0.16dB	0.030×0.122

f_m-the frequency of the transmission band

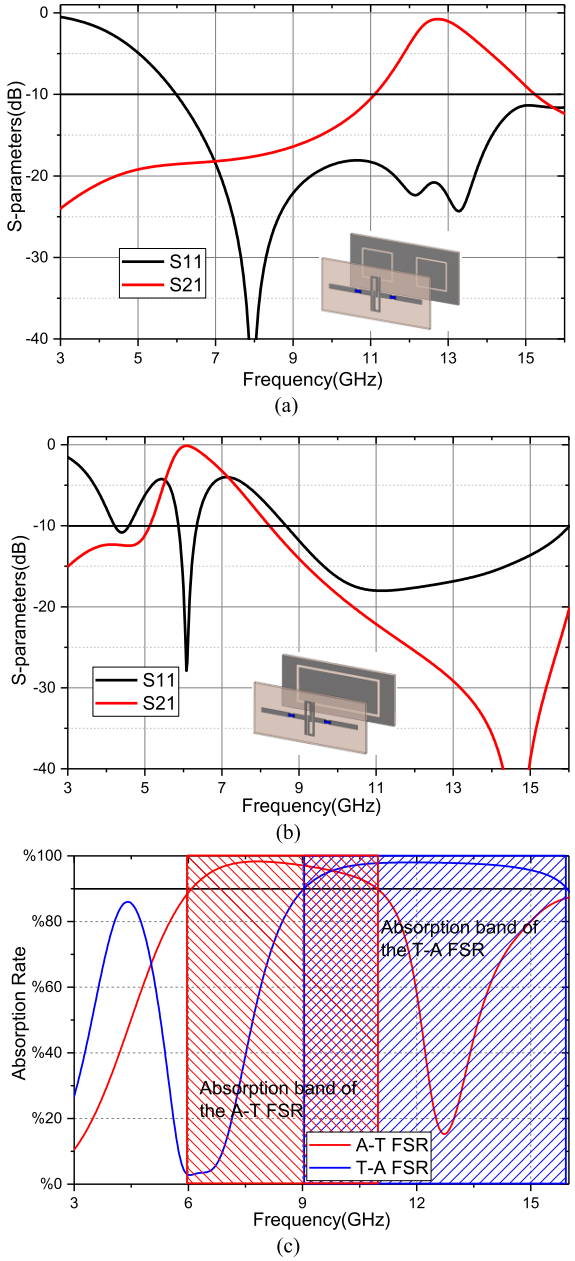

FIGURE 7. (a) Reflection and transmission coefficients of the A-T FSR using CBSR. (b) Reflection and transmission coefficients of the T-A FSR using M-CBSR. (c) Absorption rate of the proposed FSRs.

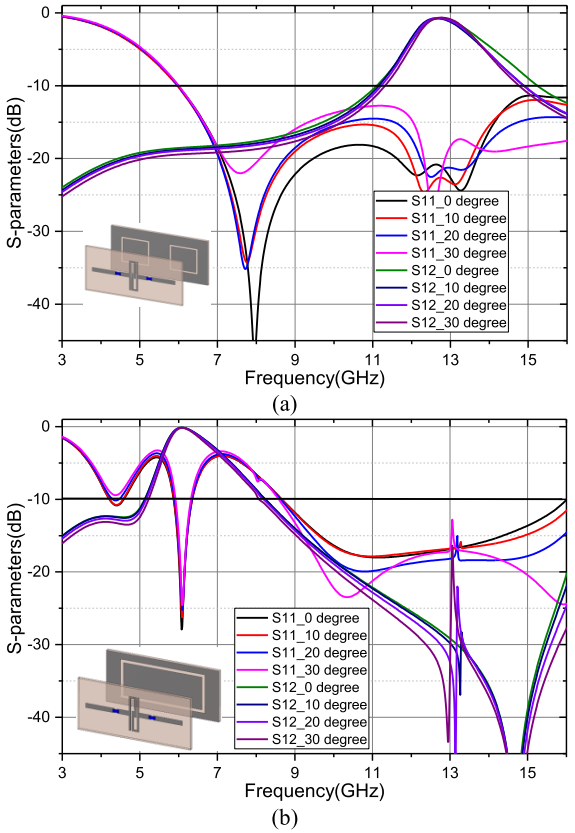

FIGURE 8. Reflection and transmission coefficients of the proposed FSRs under different oblique incidence angles. (a) A-T FSR. (b) T-A FSR.

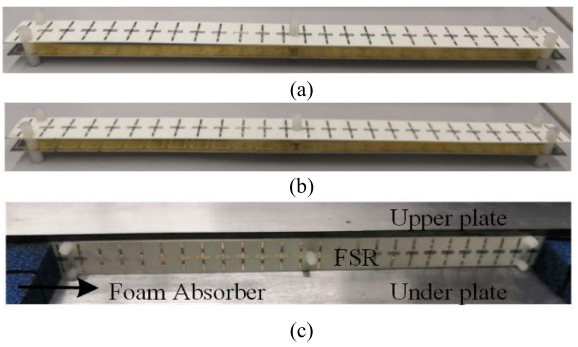

FIGURE 9. (a) Fabricated A-T FSR using CBSR. (b) Fabricated T-A FSR using M-CBSR. (c) The proposed FSR in the PPW.

Table.1 shows the performance comparison of the proposed FSRs with other FSRs in published literatures. It shows that the size of the CBSR's longer side is about one fourth of the transmission band. Comparing with the CBSR structure, the electric length of the M-CBSR's longer side is reduced about 50%, which is only 12.2% of the wavelength of the

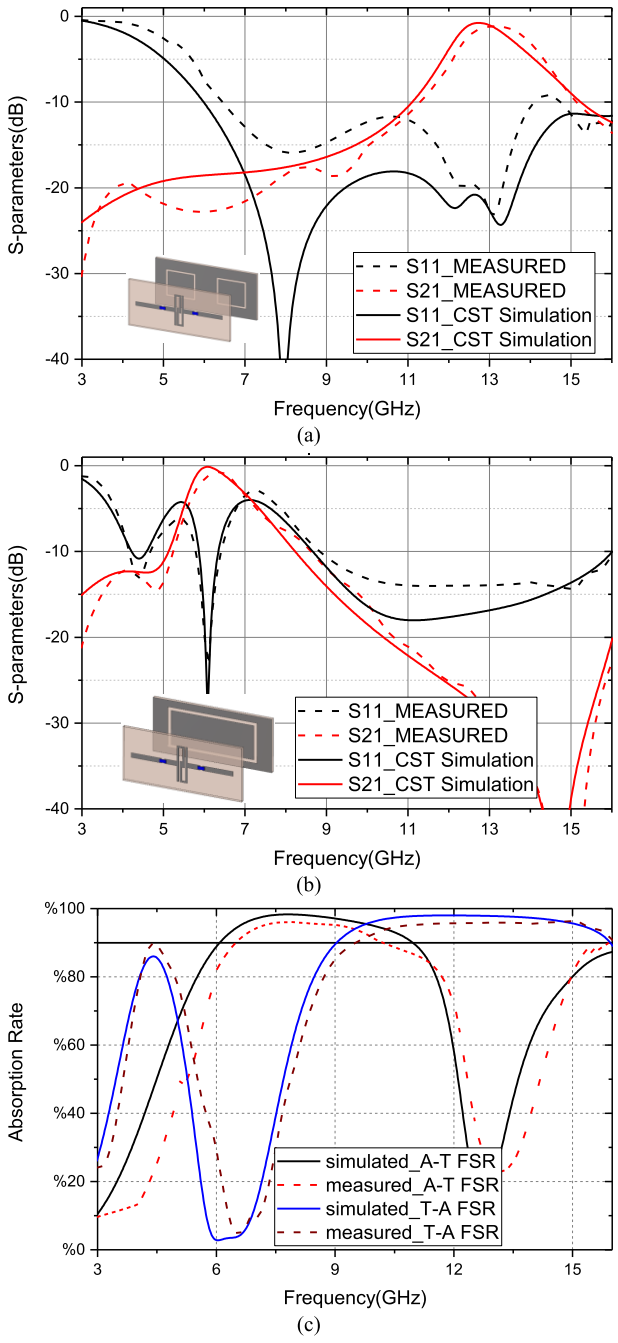

FIGURE 10. **(a) Measured and simulated transmission and reflection coefficients of the A-T FSR. (b) Measured and simulated transmission and reflection coefficients of the T -A FSR. (c) Measured and simulated absorption rate of two kinds FSRs.**

transmission band. Comparing with other resonators using different resonance structure, the resonance frequency of the proposed M-CBSR could shift to the lower frequency without enlarging the CBSR. Meanwhile, it should be noted that the insertion loss of the proposed T-A FSR is only 0.16dB, which is minimal compared with other FSRs in Table.1.

V. MEASUREMENT RESULTS

To verify the performance of the proposed FSRs, the prototypes were fabricated and measured using PPW. Fig.9 (a) and (b) show photographs of the FSRs prototypes. The resistive sheet layers and bandpass FSSs are printed on a 0.508mm-thick dielectric substrate Rogers 4350B ($\varepsilon_r = 3.48$). Chip resistors with the 0402 package were soldered on the metallic strips. Two-layer structures are fixed by five Nylon screws. Each fabricated FSR has 1×26 unit cells, the whole size is $234 \times 18\text{mm}^2$.

A PPW measurement setup is used to measure the transmission and reflection performance of the proposed FSRs [17]. In Fig.9(c), the upper plate of the PPW is removed to show the configuration of the FSRs in the PPW. An Agilent N5224A vector network analyzer (VNA) is used for the measurements. The transverse electromagnetic (TEM) wave with vertical polarization in PPW is generated by two conical disks located at both ends of PPW. The upper limit of PPW working frequency is 16 GHz. Hence, all simulated and measured results' upper limit frequency is 16GHz. To avoid multiple reflections from PPW edges, the foam absorbers are filled in the area around the edges.

Fig.10 (a) and (b) shows the measured and simulated transmission and reflection coefficients of the FSRs prototypes under the normal incidence. It is cleared that the measured and simulated results are in reasonable agreement. The small discrepancies between the measured and simulated results are attributed to the fabricated and measurement errors. As parametric parameters of the lumped resistors and solder are not taken into consideration. The measured and simulated absorption performance exists the perceptible difference. Moreover, the measured results show that two transmission bands are located at 13.09 GHz and 6.38 GHz with insertion loss of 0.74 dB and 1.16 dB, respectively. The measured and simulated absorption rates of two kinds FSRs are shown in Fig.10 (c). The A-T FSR absorption band with absorption rate $> 90\%$ extends from 6.47 GHz to 10.20 GHz, and the T-A FSR absorption band with absorption rate $> 90\%$ extend from 9.5 GHz to 16.0 GHz.

VI. CONCLUSION

This paper proposed two FSRs using CBSR and M-CBSR. One belongs to A-T FSR. The other belongs to T-A FSR. A detailed analysis of the ECMs proposed for the resistive sheet layer using CBSR and M-CBSR has been introduced. Comparing with the previous resonators using bended-strip resonance structure, the length of the M-CBSR's longer side is minimum, which is only 12.2% of the wavelength of the transmission band. Comparing with other FSRs using different resonance structures, the resonance frequency of the proposed M-CBSR could shift to the lower frequency without enlarging the CBSR. The transmission band of the proposed FSR could be shifted from high frequency to low frequency, $f_H = 2.15 f_L$. FSRs prototypes are fabricated and measured. Simulated and measured results are found in reasonable agreements. Thereby it evidently demonstrates the validity of the proposed design strategies.

REFERENCES

[1] B. A. Munk, *Frequency Selective Surfaces: Theory and Design*. New York, NY, USA: Wiley, 2000.
[2] C. Mias, "Varactor-tunable frequency selective surface with resistive-lumped-element biasing grids," *IEEE Microw. Wireless Compon. Lett.*, vol. 15, no. 9, pp. 570–572, Sep. 2005.
[3] J. Li, Q. Zeng, R. Liu, and T. A. Denidni, "A gain enhancement and flexible control of beam numbers antenna based on frequency selective surfaces," *IEEE Access*, vol. 6, pp. 6082–6091, 2018.
[4] B. A. Munk, *Metamaterials: Critique and Alternatives*, vol. 556. Hoboken, NJ, USA: Wiley, 2009.
[5] A. Motevasselian and B. L. G. Jonsson, "Design of a wideband rasorber with a polarisation-sensitive transparent window," *IET Microw., Antennas Propag.*, vol. 6, no. 7, pp. 747–755, May 2102.
[6] F. Costa and A. Monorchio, "A frequency selective radome with wideband absorbing properties," *IEEE Trans. Antennas Propag.*, vol. 60, no. 6, pp. 2740–2747, Jun. 2012.
[7] Q. Chen, J. J. Bai, L. Chen, and Y. Q. Fu, "A miniaturized absorptive frequency selective surface," *IEEE Antennas Wireless Propag. Lett.*, vol. 14, pp. 80–83, 2015.
[8] Q. Chen, S. Yang, J. Bai, and Y. Fu, "Design of absorptive/transmissive frequency-selective surface based on parallel resonance," *IEEE Trans. Antennas Propag.*, vol. 65, no. 9, pp. 4897–4902, Sep. 2017.
[9] Q. Chen, L. Chen, J. Bai, and Y. Fu, "Design of absorptive frequency selective surface with good transmission at high frequency," *Electron. Lett.*, vol. 51, no. 12, pp. 885–886, Jun. 2015.
[10] Z. Wang *et al.*, "A high-transmittance frequency-selective rasorber based on dipole arrays," *IEEE Access* vol. 6, pp. 31367–31374, 2018.
[11] H. Huang and Z. Shen, "Absorptive frequency-selective transmission structure with square-loop hybrid resonator," *IEEE Antennas Wireless Propag. Lett.*, vol. 16, pp. 3212–3215, 2017.
[12] X. Xiu, W. Che, Y. Han, and W. Yang, "Low-profile dual-polarization frequency-selective rasorbers based on simple-structure lossy cross-frame elements," *IEEE Antennas Wireless Propag. Lett.*, vol. 17, no. 6, pp. 1002–1005, Jun. 2018.
[13] K. Zhang, W. Jiang, and S. Gong, "Design bandpass frequency selective surface absorber using LC resonators," *IEEE Antennas Wireless Propag. Lett.*, vol. 16, pp. 2586–2589, 2017.
[14] Y. Han, W. Che, X. Xiu, W. Yang, and C. Christopoulos, "Switchable low-profile broadband frequency-selective rasorber/absorber based on slot arrays," *IEEE Trans. Antennas Propag.*, vol. 65, no. 12, pp. 6998–7008, Dec. 2017.
[15] Q. Chen, D. Sang, M. Guo, and Y. Fu, "Frequency-selective rasorber with interabsorption band transparent window and interdigital resonator," *IEEE Trans. Antennas Propag.*, vol. 66, no. 8, pp. 4105–4114, Aug. 2018.
[16] I. J. Bahl, *Lumped Elements for RF and Microwave Circuits*. Norwood, MA, USA: Artech House, 2003.
[17] Y. Shang, Z. Shen, and S. Xiao, "On the design of single-layer circuit analog absorber using double-square-loop array," *IEEE Trans. Antennas Propag.*, vol. 61, no. 12, pp. 6022–6029, Dec. 2013.

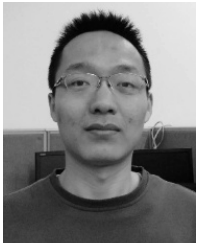

MIN GUO received the B.Eng. degree from Xidian University, Xi'an, China, in 2014, and the B.S. degree from the National University of Defense Technology, Changsha, China, in 2016, where he is currently pursuing the Ph.D. degree in microwave and millimeter wave technology. His research interests include the design of frequency-selective surface and frequency-selective rasorbers.

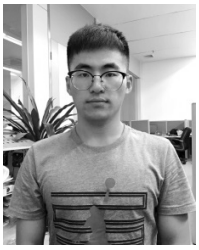

ZHANSHAN SUN received the B.S. degree from the National University of Defense Technology, Changsha, China, in 2017, where he is currently pursuing the Ph.D. degree in microwave and millimeter wave technology.

His research interests include the design of microstrip antenna, frequency-selective rasorbers, and transition metal sulfide.

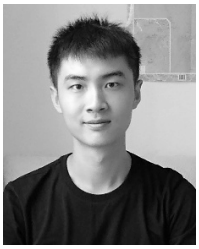

DI SANG received the bachelor's Diploma degree from the National University of Defense Technology, Hunan, China, in 2017, where he is currently pursuing the Ph.D. degree in electronic engineering. His research interests include the design of radar absorbing material, frequency-selective surfaces, artificial magnetic conductor, and periodic structures.

XUEQING JIA was born in Tianjin, China, in 1981. He received the B.Eng. and M.Sc. degrees from the National University of Defense Technology, Changsha, China, in 2003 and 2005, respectively, where he is currently pursuing the Ph.D. degree. His current research interests include artificial electromagnetic materials, circuit analog absorbers, and frequency-selective surface.

YUNQI FU received the B.Eng., M.Sc., and Ph.D. degrees in electronic science and technology from the National University of Defense Technology, Hunan, China, in 1997, 2000, and 2004, respectively. His Ph.D. Dissertation was awarded with the National Excellent Dissertation Nomination Paper and Provincial Excellent Doctoral Dissertation of Hunan.

From 2009 to 2010, he was a Visiting Scholar with The Ohio State University, Columbus, OH, USA. Since 2011, he has been a Professor with the National University of Defense Technology. He has authored or co-authored more than 100 journal papers and three books. He was elected in New Century Talent Supporting Project by Education Ministry in 2008. He has conducted three NSFC projects and more than ten other projects.

His current research interests include the artificial electromagnetic metamaterial, microwave and millimeter-wave detection and imaging.